

Observation of a topological 3D Dirac semimetal phase in high-mobility Cd₃As₂

M. Neupane^{*,1,2} S.-Y. Xu^{*,1} R. Sankar^{*,3} N. Alidoust^{,1} G. Bian,¹ Chang Liu,¹ I. Belopolski,¹ T.-R. Chang,⁴ H.-T. Jeng,^{4,5} H. Lin,⁶ A. Bansil,⁷ Fangcheng Chou,³ and M. Z. Hasan^{1,8}

¹Joseph Henry Laboratory, Department of Physics,
Princeton University, Princeton, New Jersey 08544, USA

²Princeton Center for Complex Materials, Princeton University, Princeton, New Jersey 08544, USA

³Center for Condensed Matter Sciences, National Taiwan University, Taipei 10617, Taiwan

⁴Department of Physics, National Tsing Hua University, Hsinchu 30013, Taiwan

⁵Institute of Physics, Academia Sinica, Taipei 11529, Taiwan

⁶Graphene Research Centre and Department of Physics,
National University of Singapore 11754, Singapore

⁷Department of Physics, Northeastern University, Boston, Massachusetts 02115, USA

⁸Princeton Center for Complex Materials, PRISM,
Princeton University, Princeton, New Jersey 08544, USA

(Dated: 25 September, 2013)

Experimental identification of three-dimensional (3D) Dirac semimetals in solid state systems is critical for realizing exotic topological phenomena and quantum transport such as the Weyl phases, high temperature linear quantum magnetoresistance and topological magnetic phases. Using high resolution angle-resolved photoemission spectroscopy, we performed systematic electronic structure studies on well-known compound Cd₃As₂. For the first time, we observe a highly linear bulk Dirac cone located at the Brillouin zone center projected onto the (001) surface which is consistent with a 3D Dirac semimetal phase in Cd₃As₂. Remarkably, an unusually high Dirac Fermion velocity up to 10.2 Å·eV ($\approx 1.6 \times 10^6$ ms⁻¹) is seen in samples where the mobility far exceeds 20,000 cm²/V.s suggesting that Cd₃As₂ can be a promising candidate as a hypercone analog of graphene in many device-applications which can also incorporate topological quantum phenomena in a large gap setting. Our experimental identification of this novel topological 3D Dirac semimetal phase, distinct from a 3D topological insulator phase discovered previously, paves the way for exploring higher dimensional relativistic physics in bulk transport and for realizing novel fermionic matter such as a Fermi arc nodal metal.

Two-dimensional (2D) Dirac electron systems often exhibit exotic quantum phenomena, and therefore have been considered as one of the central topics in modern condensed matter physics [1–8]. The most notable examples are the extensive studies on graphene and the surface states of topological insulators (TI). Three-dimension (3D) Dirac fermions, sometimes noted as the bulk Dirac semimetals (BDS) phase, are also of great research interest because its 3D relativistic dispersion can lead to peculiar and novel physical properties. For example, unusual electrical and thermal transport phenomena have been observed in the massive Dirac bands in bulk bismuth [9]. More interestingly, the BDS state is also believed to be the key to realizing exotic Weyl physics [1, 10–17]. It has been theoretically understood that a BDS can be viewed as a composite of two sets of Weyl fermions [10, 13]. And furthermore if time-reversal or space inversion symmetry is broken, theory predicts that the 3D Dirac point can split into two Weyl nodes that are separated in momentum space, thus realizing a Weyl semimetal phase.

In spite of the predicted exotic properties, experimental studies on the *massless* BDS phase have been lacking, because it is found to be challenging to experimentally realize the BDS state in real material, especially in stoichiometric single crystalline systems. It has been shown

that the BDS state can be achieved at the critical point of a topological phase transition between a normal insulator and a topological insulator [18]. However, such approach requires very fine-tuning of the chemical doping/alloying composition (effectively the spin-orbit coupling strength), which is difficult to control and also introduces chemical disorder limiting the mobility of the system. On the other hand, in stoichiometric bulk materials, bismuth is a known example but Dirac fermions in bismuth are in fact massive (there exists a mass gap in the bulk Dirac spectrum) [5, 9]. Therefore, to this date, identification of BDS phase in stoichiometric materials, especially with high transport electron mobility critical for transport and device applications, remains experimentally elusive.

In this letter, we present our experimental identification of a Dirac semimetal phase in stoichiometric single crystalline system of Cd₃As₂, which is protected by the C₄ crystalline symmetry. Using high-resolution angle-resolved photoemission spectroscopy (ARPES), we show that Cd₃As₂ features a bulk band Dirac cone locating at the center of the (001) surface Brillouin zone (BZ). Remarkably, we observe the band velocity of the bulk Dirac spectrum in Cd₃As₂ to be as high as 10.2 Å·eV, which is highly favorable for realizing the high mobility

($10^5 \text{ cm}^2\text{V}^{-1}\text{s}^{-1}$ [19]) in transport studies. We further briefly compare and contrast the observed crystalline-symmetry-protected BDS phase in Cd_3As_2 with those of in the Bi-based 3D-TI systems such as in $\text{BiTi}(\text{S}_{1-\delta}\text{Se}_\delta)_2$ and $(\text{Bi}_{1-\delta}\text{In}_\delta)_2\text{Se}_3$ systems, which are realized by tuning δ to the critical point of a topological phase transition. Our observation of the bulk Dirac semimetal phase in stoichiometric Cd_3As_2 with a very high Fermi velocity in combination with large electron mobility opens the door for observing exotic 3D Dirac relativistic physics in bulk materials and for realizing the Fermi arc semimetal topological phases.

Single crystalline samples of Cd_3As_2 were grown using the standard method, which is described elsewhere [23]. ARPES measurements for the low energy electronic structure were performed at the PGM beamline in Synchrotron Radiation Center (SRC) in Wisconsin, and at the beamlines 4.0.3 and 10.0.1 at the Advanced Light Source (ALS) in Berkeley California, equipped with high efficiency VG-Scienta R4000 and R8000 electron analyzers. Samples were cleaved *in situ* and measured at 10–80 K in a vacuum better than 1×10^{-10} torr. They were found to be stable and without degradation for the typical measurement period of 20 hours. Based on the experimentally determined parameters we recalculate the band-structure of this system which was not available while previous calculations were done [12]. Our first-principles calculations are based on the generalized gradient approximation (GGA) [20] using the projector augmented wave method [21] as implemented in the VASP package [22]. The experimental data for the crystal structure were performed over $4 \times 4 \times 2$ Monkhorst-Pack k -mesh with the spin-orbit coupling included self-consistently.

The crystal structure of Cd_3As_2 has a tetragonal unit cell with $a = 12.67 \text{ \AA}$, $c = 25.48 \text{ \AA}$, $Z = 32$, and the space group of $I4_1cd$ (see Figs. 1a and b). In this structure, arsenic ions are approximately cubic close-packed and Cd ions are tetrahedrally coordinated. Each As ion is surrounded by Cd ions at six of the eight corners of a distorted cube (see Fig. 1b), with the two vacant sites being at diagonally opposite corners of a cube face [23]. The corresponding Brillouin zone (BZ) is shown in Fig. 1d, where the center of the BZ is the Γ point, the centers of the top and bottom square surfaces are the Z points, and other high symmetry points are also noted. In electrical transport measurements, Cd_3As_2 has long attracted much attention because of its very high electron mobility up to $\simeq 10^5 \text{ cm}^2\text{V}^{-1}\text{s}^{-1}$ [19] and interesting magneto-transport properties including a very small effective mass [24]. In band theoretical calculations, Cd_3As_2 is also of interests because it is believed to have an inverted band structure [25]. More interestingly, a very recent theoretical study [13] has shown that the spin-orbit interaction in Cd_3As_2 cannot open up a full energy gap between the inverted bulk conduction and valence bands due to

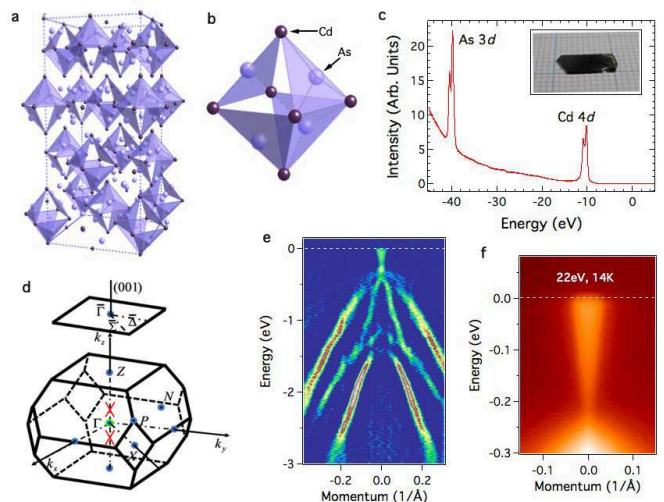


FIG. 1: **a**, Cd_3As_2 crystallizes in a tetragonal body center structure with space group of $I4_1cd$, which has 32 number of formula units in the unit cell. The tetragonal structure has lattice constant of $a = 12.670 \text{ \AA}$, $b = 12.670 \text{ \AA}$, and $c = 25.480 \text{ \AA}$. **b**, The basic structure unit is a 4 corner-sharing CdAs_3 -trigonal pyramid. **c**, Core-level spectroscopic measurement where Cd $4d$ and As $3d$ peaks are clearly observed. Inset shows a picture of the Cd_3As_2 samples used for ARPES measurements. The flat and mirror-like surface indicates the high quality of our samples. **d**, The bulk Brillouin zone (BZ) and the projected surface BZ along the (001) direction. The red crossings locate at $(k_x, k_y, k_z) = (0, 0, 0.15 \frac{2\pi}{c^*})$ ($c^* = c/a$). They denote the two special \mathbf{k} points along the $\Gamma - Z$ momentum space cut-direction, where 3D Dirac band-touchings are protected by the crystalline C_4 symmetry along the k_z axis. **e**, Second derivative image of ARPES dispersion map of Cd_3As_2 over the wider binding energy range. Various bands are well-resolved up to 3 eV binding energy range. **f**, ARPES $E_B - k_x$ cut of Cd_3As_2 near the Fermi level at around surface BZ center $\bar{\Gamma}$ point. Additional data are shown in the Supplementary Information section.

the protection of an additional crystallographic symmetry [11] (in the case of Cd_3As_2 it is the C_4 rotational symmetry along the k_z direction [13]), which is in contrast to other band-inverted systems such as Bi_2Se_3 or HgTe [3]. Theory predicts [13] that the C_4 rotational symmetry protects two bulk (3D) Dirac band touchings at two special \mathbf{k} points along the $\Gamma - Z$ momentum space cut-direction, as shown by the red crossings in Fig. 1d. Therefore, Cd_3As_2 serves a candidate for an exotic space group symmetry-protected bulk Dirac semimetal (BDS) phase, which additionally feature a high carrier mobility and an inverted band-structure.

In order to experimentally identify such exotic BDS phase, we systematically study the electronic structure of Cd_3As_2 at the cleaved (001) surface. Fig. 1c shows momentum-integrated ARPES spectral intensity over a wide energy window. Sharp ARPES intensity peaks at binding energies of $E_B \simeq 11 \text{ eV}$ and 41 eV corresponding to the cadmium $4d$ and the arsenic $3d$ core levels

are observed, confirming the correct chemical composition of our samples. We now study the overall electronic structure of the valence band. Fig. 2e shows the second derivative image of an ARPES dispersion map in a 3 eV binding energy window (the corresponding raw data is shown in the supplementary information (SI)), where the dispersion of several valence bands are clearly identified. Moreover, a low-lying small feature that crosses the Fermi level is observed. In order to resolve it, high-resolution ARPES dispersion measurements are performed in the close vicinity of the Fermi level shown in Fig. 1f. Remarkably, a linearly dispersive Dirac cone is observed at the surface BZ center $\bar{\Gamma}$ point, whose Dirac node is found to locate at binding energy of $E_B \simeq 0.2$ eV. At the Fermi level, only the upper Dirac band but no other electronic states are observed. On the other hand, the lower Dirac cone is found to coexist with a parabolic bulk valence band, which can be seen from Fig. 1e. We compare our ARPES observation with our theoretical calculations (our theoretical calculations are consistent with the earlier results reported in Ref. [13] but optimized based on data taken on the samples used in our experiments). In theory, there are two 3D Dirac nodes that are expected at two special \mathbf{k} points along the $\Gamma - Z$ momentum space cut-direction, as shown by the red crossings in Fig. 1d. At the (001) surface, these two \mathbf{k} points along the $\Gamma - Z$ axis both project on to the $\bar{\Gamma}$ point of the (001) surface BZ (Fig. 1d). Therefore, at the (001) surface, theory predicts one 3D Dirac cone at the BZ center $\bar{\Gamma}$ point, as shown in Fig. 2a. These results are in qualitative agreement with our data, which supports our experimental observation of the 3D BDS phase in Cd_3As_2 . We also study the ARPES measured constant energy contour maps as shown in Fig. 2e and f. At the Fermi level, the constant energy contour is a single pocket centered at the $\bar{\Gamma}$ point. As increasing the binding energy, the size of the pocket decreases and eventually shrinks to a point (the 3D Dirac point) at binding energy of $E_B \simeq 0.2$ eV.

We compare the ARPES data on Cd_3As_2 with the prototype TI Bi_2Se_3 , to highlight the distinct nature of the surface electronic structure of the 3D BDS phase in Cd_3As_2 . As shown in Fig. 3b, in TI Bi_2Se_3 , the bulk conduction and valence bands are fully separated (gapped), and a linearly dispersive topological surface state connects the bulk band-gap. In case of Cd_3As_2 (Fig. 3a), there does not exist a full bulk energy gap. On the other hand, the bulk conduction and valence bands “touch” (and only “touch”) at one specific location in the momentum space, which is the 3D Dirac point, thus realizing a 3D BDS. We further show that the BDS state can also be realized by tuning the chemical composition δ (effectively the spin-orbit coupling strength) to the critical point of a topological phase transition between a normal insulator and a topological insulator [18, 29]. Fig. 3 presents the surface electronic structure of two other

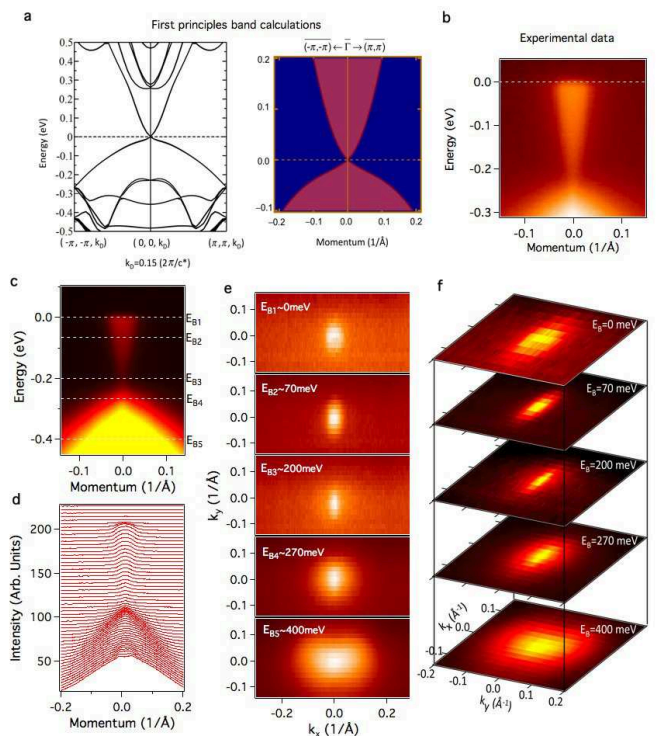


FIG. 2: Observation of 3D bulk Dirac cone in Cd_3As_2 . **a**, Left: First principles calculation of the bulk electronic structure along the $(\pi, \pi, 0.15\frac{2\pi}{c^*}) - (0, 0, 0.15\frac{2\pi}{c^*})$ direction ($c^* = c/a$). A 3D bulk Dirac band is found in our calculation. Right: Slab calculation projected at the (001) surface, where the shaded area shows the projection of the bulk bands. **b** and **c** ARPES measured dispersion map of Cd_3As_2 , measured with photon energy of 22 eV and temperature of 15 K along the $(-\pi, -\pi) - (0, 0) - (\pi, \pi)$ momentum space cut-direction. Dashed lines denote the binding energies of the constant energy contours shown in Panel (e). **d**, Momentum distribution curves (MDCs) of the spectrum presented in **b**. **e** and **f** APRES measured constant energy contours. The binding energies are noted on the plots. Additional data are shown in the Supplementary Information section.

BDS phases in the $\text{BiTl}(\text{S}_{1-\delta}\text{Se}_\delta)_2$ and $(\text{Bi}_{1-\delta}\text{In}_\delta)_2\text{Se}_3$ systems. In both systems, it has been shown that tuning the chemical composition δ can drive the system from a normal insulator state to a topological insulator state [18, 29]. The critical composition for the two topological phase transitions is near 50% and 4%, respectively. Fig. 3c and d show the ARPES measured surface electronic structure of the critical compositions for both $\text{BiTl}(\text{S}_{1-\delta}\text{Se}_\delta)_2$ and $(\text{Bi}_{1-\delta}\text{In}_\delta)_2\text{Se}_3$ systems, which are expected to exhibit the BDS phase. Indeed, the critical compositions also show Dirac cones with intensities filled inside the cones, which is qualitatively similar to the case in Cd_3As_2 . From the observed steep Dirac dispersion in Cd_3As_2 , we obtain a surprisingly high Fermi velocity of about $10.2 \text{ eV}\cdot\text{\AA} (\simeq 1.6 \times 10^6 \text{ ms}^{-1})$. Comparing to the much-studied 2D Dirac systems, the Fermi

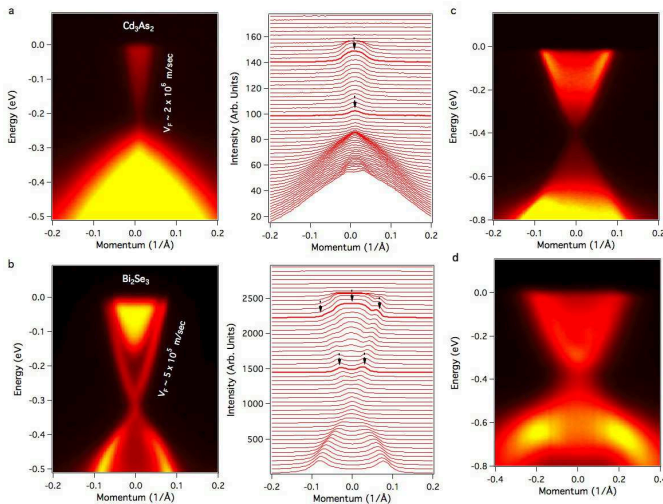


FIG. 3: Comparison of the surface electronic structure of 2D and 3D Dirac fermions. (a) ARPES measured surface electronic structure dispersion map of Cd_3As_2 and its corresponding momentum distribution curves (MDCs). (b) ARPES measured surface dispersion map of the prototype TI Bi_2Se_3 and its corresponding momentum distribution curves. Both spectra are measured with photon energy of 22 eV and at a sample temperature of 15 K. The black arrows show the ARPES intensity peaks in the MDC in the MDC plots. (c) and (d) ARPES spectra of two 3D Dirac semimetals, which are realized by fine tuning the chemical composition to the critical point of a topological phase transition between a normal insulator and a TI [18, 29]: (c) $\text{TlBi}(\text{S}_{1-\delta}\text{Se}_\delta)_2$ ($\delta = 0.5$), and (d) $(\text{Bi}_{1-\delta}\text{In}_\delta)_2\text{Se}_3$ ($\delta = 0.04$). Spectrum in (c) is measured with photon energy of 16 eV and spectrum in (d) is measured with photon energy of 41 eV. For the 2D topological surface Dirac cone in Bi_2Se_3 , a distinct in-plane ($E_B - k_x$) dispersion is observed in ARPES, whereas for the 3D bulk Dirac cones in Cd_3As_2 , $\text{TlBi}(\text{S}_{0.5}\text{Se}_{0.5})_2$, and $(\text{Bi}_{0.96}\text{In}_{0.04})_2\text{Se}_3$, a Dirac-cone-like intensity continuum is observed. Additional data are shown in the Supplementary Information section.

velocity of the 3D Dirac fermions in Cd_3As_2 is about 3 times higher than that of in the topological surface states (TSS) of Bi_2Se_3 [6], 1.5 times higher than in graphene [26] and 30 times higher than the theoretically calculated TSS in the topological Kondo insulator phase in SmB_6 [27]. The observed large Fermi velocity of the 3D Dirac band contributes to factors that make Cd_3As_2 a high mobility medium in transport experiments [19]. Therefore one can expect to observe exotic magneto-electrical and thermal transport properties under high magnetic field. It is well-known that in graphene the ability to prepare high quality and high mobility samples has enabled the experimental observations of many interesting physics that arises from its 2D Dirac fermions. Therefore, the large Fermi velocity and high mobility in Cd_3As_2 serve as a remarkable combination of experimental conditions in order to systematically explore the 3D Dirac relativistic physics in Cd_3As_2 .

In conclusion, we have experimentally identified the

first crystalline-symmetry-protected 3D BDS phase in a stoichiometric semiconducting system Cd_3As_2 . The observed large Fermi velocity and very high electron mobility of the 3D Dirac fermion carriers in Cd_3As_2 make it an ideal platform to test novel 3D Dirac relativistic physics in solid-state settings. Our first observation of a 3D BDS phase also paves the way for realizing a number of exotic topological phenomena. For example, if the C_4 crystalline symmetry is broken, the 3D Dirac cone in Cd_3As_2 can open up a gap and therefore a topological insulator phase is realized in a high mobility setting. Also, upon doping magnetic elements or fabricating superlattice structure, the 3D Dirac node in Cd_3As_2 can be split into two topologically protected Weyl nodes, realizing the Weyl topological phase with spin-momentum locked Fermi arcs on the surfaces which is expected to exhibit large linear magnetoresistance.

*These authors contributed equally to the project.

Correspondence should be addressed to M.Z.H. (Email: mzhasan@princeton.edu).

-
- [1] H. Weyl, Phys. **56**, 330 (1929).
 - [2] A. K. Geim, and K. S. Novoselov, Nature Mat. **6**, 183 (2007).
 - [3] M. Z. Hasan, & C. L. Kane, Rev. Mod. Phys. **82**, 3045-3067 (2010).
 - [4] X-L. Qi & S.-C. Zhang, Rev. Mod. Phys. **83**, 1057-1110 (2011).
 - [5] D. Hsieh *et al.*, Nature **452**, 970-974 (2008).
 - [6] Y. Xia *et al.*, Nature Phys. **5**, 398-402 (2009).
 - [7] D. Hsieh, *et al.* A tunable topological insulator in the spin helical Dirac transport regime. Nature **460**, 1101-1105 (2009).
 - [8] Y. L. Chen *et al.*, Science **325**, 178-181 (2010).
 - [9] L. Li *et al.*, Science **321**, 547 (2008).
 - [10] S. Murakami, New. J. Phys. **9**, 356 (2007).
 - [11] S. M. Young *et al.*, Phys. Rev. Lett. **108**, 140405 (2012).
 - [12] Z. Wang *et al.*, Phys. Rev. B **85**, 195320 (2012).
 - [13] Z. Wang *et al.*, arXiv: 1305.6780 (2013).
 - [14] G. T. Volovik, JETP Lett. **75**, 55 (2002).
 - [15] Z. Fang, N. Nagaosa, K. S. Takahashi *et al.*, Science **302**, 92 (2003).
 - [16] X. Wan *et al.*, Phys. Rev. B **83**, 205101 (2011).
 - [17] G. B. Halasz, L. Balents, Phys. Rev. B. **85** 035103 (2012).
 - [18] S. Y. Xu *et al.*, Science **332**, 560-564 (2011).
 - [19] J.-P. Jay-Gerin, M.J. Aubin and L.G. Caron, Solid State Communications **21**, 771 (1977).
 - [20] J. P. Perdew, K. Burke, and M. Ernzerhof, Phys. Rev. Lett. **77**, 3865 (1996).
 - [21] P. E. Blochl, Phys. Rev. B. **50**, 17953 (1994); G. Kresse and J. Joubert, Phys. Rev. B. **59**, 1758 (1999).
 - [22] G. Kress and J. Hafner, Phys. Rev. B. **48**, 13115 (1993); G. Kress and J. Furthmuller, Comput. Mater. Sci. **6**, 15 (1996); Phys. Rev. B. **54**, 11169 (1996).
 - [23] G. A. Steigmann, and J. Goodyear, Acta Cryst. B **24**, 1062 (1968).
 - [24] W. Zdanowicz *et al.*, Thin Solid Films **61**, 41 (1979).
 - [25] B. D. Plenkiewicz and P. Plenkiewicz, Physica Status

Solidi(b) **94**, K57 (2006).

- [26] A. Bostwick *et al.*, Nature Phys. **3**, 36 (2007).
 [27] F. Lu, *et al.*, Phys. Rev. Lett. **110**, 096401 (2013).
 [28] L. A. Wray *et al.*, Phys. Rev. B **83**, 224516 (2011).
 [29] M. Brahlek *et al.*, Phys. Rev. Lett. **109**, 186403 (2012).

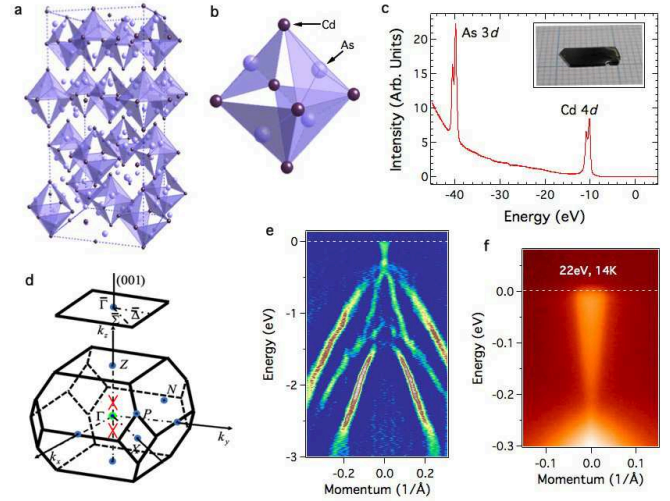


FIG. 4: **Sample characterization.** **a**, Cd_3As_2 crystallizes in a tetragonal body center structure with space group of $I4_1cd$, which has 32 number of formula units in the unit cell. The tetragonal structure has lattice constant of $a = 12.670 \text{ \AA}$, $b = 12.670 \text{ \AA}$, and $c = 25.480 \text{ \AA}$. **b**, The basic structure unit is a 4 corner-sharing CdAs_3 -trigonal pyramid. **c**, Core-level spectroscopic measurement where $\text{Cd } 4d$ and $\text{As } 3d$ peaks are clearly observed. Inset shows a picture of the Cd_3As_2 samples used for ARPES measurements. The flat and mirror-like surface indicates the high quality of our samples. **d**, The bulk Brillouin zone (BZ) and the projected surface BZ along the (001) direction. The red crossings locate at $(k_x, k_y, k_z) = (0, 0, 0.15 \frac{2\pi}{c^*})$ ($c^* = c/a$). They denote the two special \mathbf{k} points along the $\Gamma - Z$ momentum space cut-direction, where 3D Dirac band-touchings are protected by the crystalline C_4 symmetry along the k_z axis. **e**, Second derivative image of ARPES dispersion map of Cd_3As_2 over the wider binding energy range. Various bands are well-resolved up to 3 eV binding energy range. **f**, ARPES $E_B - k_x$ cut of Cd_3As_2 near the Fermi level at around surface BZ center $\bar{\Gamma}$ point. Additional data are shown in the Supplementary Information section.

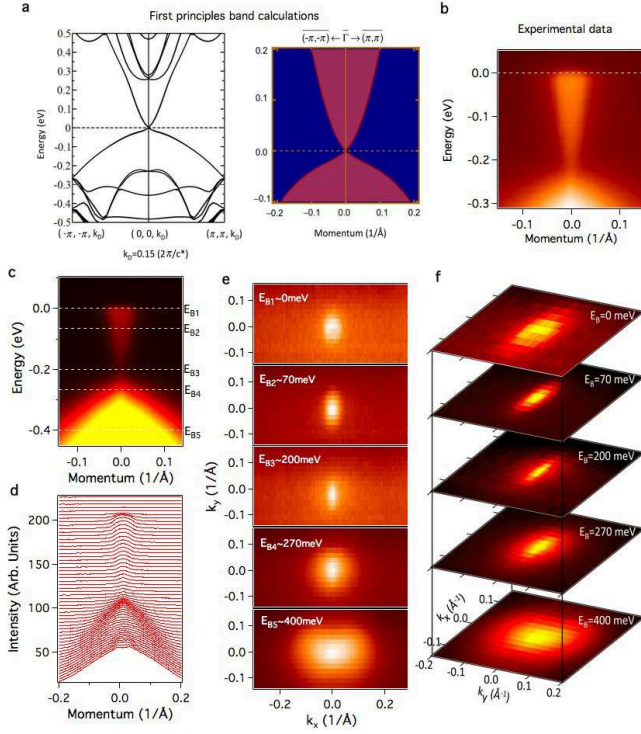


FIG. 5: Observation of 3D bulk Dirac cone in Cd_3As_2 . **a**, Left: First principles calculation of the bulk electronic structure along the $(\pi, \pi, 0.15 \frac{2\pi}{c^*}) - (0, 0, 0.15 \frac{2\pi}{c^*})$ direction ($c^* = c/a$). A 3D bulk Dirac band is found in our calculation. Right: Slab calculation projected at the (001) surface, where the shaded area shows the projection of the bulk bands. **b** and **c** ARPES measured dispersion map of Cd_3As_2 , measured with photon energy of 22 eV and temperature of 15 K along the $(-\pi, -\pi) - (0, 0) - (\pi, \pi)$ momentum space cut=direction. Dashed lines denote the binding energies of the constant energy contours shown in Panel (e). **d**, Momentum distribution curves (MDCs) of the spectrum presented in **b**. **e** and **f** APRES measured constant energy contours. The binding energies are noted on the plots. Additional data are shown in the Supplementary Information section.

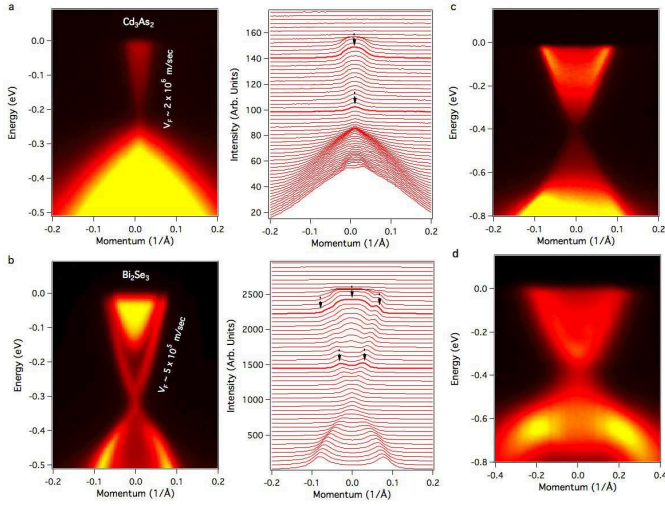


FIG. 6: Comparison of the surface electronic structure of 2D and 3D Dirac fermions. (a) ARPES measured surface electronic structure dispersion map of Cd₃As₂ and its corresponding momentum distribution curves (MDCs). (b) ARPES measured surface dispersion map of the prototype TI Bi₂Se₃ and its corresponding momentum distribution curves. Both spectra are measured with photon energy of 22 eV and at a sample temperature of 15 K. The black arrows show the ARPES intensity peaks in the MDC in the MDC plots. (c and (d)) ARPES spectra two 3D Dirac semimetals, which are realized by fine tuning the chemical composition to the critical point of a topological phase transition between a normal insulator and a TI [18, 29?]: (c) TlBi(S_{1- δ} Se _{δ})₂ ($\delta = 0.5$), and (Bi_{1- δ} In _{δ})₂Se₃ ($\delta = 0.04$) (d). Spectrum in (c) is measured with photon energy of 16 eV and spectrum in (d) is measured with photon energy of 41 eV. For the 2D topological surface Dirac cone in Bi₂Se₃, a distinct in-plane ($E_B - k_x$) dispersion is observed in ARPES, whereas for the 3D bulk Dirac cones in Cd₃As₂, TlBi(S_{0.5}Se_{0.5})₂, and (Bi_{0.96}In_{0.04})₂Se₃, a Dirac-cone-like intensity continuum is observed. Additional data are shown in the Supplementary Information section.